Science Get Journal
Vol. 03, No. 2, April 2026, 53-63
e-ISSN: 3062-6595

Green-Synthesized Carbon Quantum Dots from Banana Peel Waste for Sustainable Label-Free Fluorescent Biosensing of Prostate Cancer Biomarker

Nor Pana Yupa[1]*, & Dian Putri Mustika[2]
[1]*IPB University, Indonesia, [2]Universitas Negeri Padang, Indonesia
*Co e-mail: norpanay1@gmail.com[1]

Article Information
Received: April 15, 2026
Revised: May 18, 2026
Online: May 21, 2026

Keywords
Carbon Quantum Dots, Banana Peel, Prostate-Specific Antigen (PSA), Prostate Cancer

ABSTRACT

A novel fluorescent biosensing platform for the label-free, sustainable detection of prostate-specific antigen (PSA) was developed using green-synthesized carbon quantum dots (CQDs) derived from banana peel (Musa acuminata) agricultural waste. CQDs were fabricated via a one-step hydrothermal carbonization at 200°C for 8 hours, yielding quasi-spherical nanoparticles with an average diameter of 3.2 ± 0.5 nm, a quantum yield of 18.4%, and characteristic blue emission at 460 nm (λex = 360 nm). Rich surface functionalization with hydroxyl (–OH), carboxyl (–COOH), and amino ($–NH_2$) groups enabled covalent conjugation of a PSA-specific aptamer via EDC/NHS coupling chemistry. The resulting CQD-aptamer biosensor exhibited a broad linear detection range of 0.01–50 ng/mL with an ultralow limit of detection (LOD) of 0.008 ng/mL (S/N = 3), well within the clinical diagnostic threshold of 4 ng/mL for PSA monitoring. Selectivity studies demonstrated negligible cross-reactivity (<3.5%) against common serum interferents including CEA, AFP, albumin, and glucose. Spike-and-recovery experiments in diluted human serum yielded recovery values of 96.8–103.2% with RSDs below 2.5%, confirming robust performance in complex biological matrices. Estimated material costs (~$0.12/mg CQD) and the waste-valorization approach align with green chemistry principles and circular economy objectives. This work establishes banana peel-derived CQDs as cost-effective, eco-friendly, and analytically competitive nanoprobes for point-of-care cancer biomarker detection.

Keywords: *Carbon Quantum Dots, Banana Peel, Prostate-Specific Antigen (PSA), Prostate Cancer*

http://doi.org/10.69855/science.v3i2.602
https://gpijournal.com/index.php/science
PUBLISHED BY : GPress Indonesia

INTRODUCTION

Prostate cancer ranks as the second most prevalent malignancy affecting men globally, accounting for approximately 1.4 million newly diagnosed cases and 375,000 fatalities annually (Sung et al., 2021). Early-stage detection is the single most critical determinant of patient survival: localized prostate cancer carries a five-year survival rate exceeding 99%, whereas metastatic disease drops sharply to 31% (Siegel et al., 2023). Prostate-specific antigen (PSA), a serine protease secreted by prostatic epithelial cells, is the most widely adopted serum biomarker in clinical screening programs, with a diagnostic threshold established at 4 ng/mL (Litwin & Tan, 2017).

Standard PSA quantification relies predominantly on enzyme-linked immunosorbent assay (ELISA) or chemiluminescence immunoassay (CLIA). Despite their established sensitivity, these methods are encumbered by high instrumentation costs, prolonged processing times, dependence on trained personnel, and reliance on enzymatic labels that compromise storage stability and cold-chain logistics (Zhang et al., 2022; Chen et al., 2021). These limitations have driven considerable interest in alternative sensing platforms that combine high sensitivity with operational simplicity and cost-effectiveness suitable for point-of-care (POC) settings particularly in resource-limited environments where conventional laboratory infrastructure may be unavailable.

Carbon quantum dots (CQDs) have emerged as highly promising next-generation biosensing probes over the past decade, owing to their size-tunable photoluminescence, exceptional photostability, low cytotoxicity, favorable biocompatibility, and versatile surface chemistry (Baker & Baker, 2010; Lim et al., 2015; Cayuela et al., 2016). Unlike conventional semiconductor quantum dots (e.g., CdSe, ZnS), CQDs are free from heavy-metal toxicity, rendering them substantially more appropriate for biomedical applications (Zhu et al., 2015; Devi et al., 2019).

A particularly promising direction within CQD research is the exploitation of agricultural waste streams as sustainable carbon precursors. Biomass-derived CQDs have been prepared from orange peel (Sahu et al., 2012), sugarcane bagasse (Huang et al., 2013), spent coffee grounds (Wang et al., 2023), and rice husk (Chen et al., 2022), simultaneously advancing waste valorization aligned with circular economy principles. Among these feedstocks, banana peel (Musa acuminata) is especially compelling: it is rich in carbon, bears abundant oxygen-functional groups (–OH, –COOH) inherent to its polyphenolic and cellulosic composition, and is available in vast quantities, underpinned by global annual production exceeding 120 million tonnes (FAO, 2023). Indonesia alone generates an estimated 4.5 million tonnes of banana peel waste annually, the majority of which remains underexploited (Sulaiman et al., 2022).

Label-free biosensing strategies which transduce the native optical response of the sensing material upon direct analyte binding without requiring secondary labeling are particularly well-suited to POC applications on account of their streamlined assay architectures and reduced reagent dependency (Shrivastava et al., 2022). Aptamers, single-stranded oligonucleotides that bind target proteins with high affinity through target-induced conformational changes, represent ideal molecular recognition elements for CQD-based label-free biosensors: they can be covalently conjugated to CQD surfaces and their structural rearrangement upon target binding produces measurable, concentration-dependent fluorescence modulation (Yin et al., 2020).

Despite meaningful progress in the field, the development of CQD biosensors for PSA detection that simultaneously achieve sub-nanogram sensitivity, employ green synthesis from waste-derived precursors, and demonstrate rigorous validation in clinical sample matrices remains an underexplored area. The present study addresses this gap by reporting: (a) the hydrothermal synthesis and comprehensive physicochemical characterization of highly luminescent banana peel-derived CQDs; (b) their covalent functionalization with a PSA-targeting aptamer; and (c) their deployment as a label-free fluorescence biosensor for PSA quantification in both buffer and spiked human serum. The analytical figures of merit are systematically benchmarked against previously reported CQD-based PSA sensing systems. The study further situates the approach within sustainability and translational feasibility frameworks relevant to real-world POC diagnostics.

METHODS

1. Materials and Reagents

Banana peels (Musa acuminata, Cavendish variety) were collected from a local fruit market in Pekanbaru, Indonesia, and washed thoroughly under running deionized water prior to use. Sodium hydroxide (NaOH, ≥99%), hydrochloric acid (HCl, 37%), phosphate-buffered saline (PBS), bovine serum albumin (BSA), carcinoembryonic antigen (CEA), alpha-fetoprotein (AFP), uric acid, and D-glucose were purchased from Sigma-Aldrich (St. Louis, MO, USA).

Recombinant human PSA antigen and the PSA-specific aptamer (5'-GGG TGG GTG GGT GGG T-3') were obtained from Elabscience Biotechnology (Houston, TX, USA). EDC (1-ethyl-3-(3-dimethylaminopropyl)carbodiimide hydrochloride) and NHS (N-hydroxysuccinimide) were supplied by Thermo Fisher Scientific. All solutions were prepared with ultrapure water (18.2 MΩ·cm, Milli-Q). Human serum samples were obtained with informed consent under Ethics Committee approval (Universitas Riau, Protocol No. UR-EC-2024-018).

2. Synthesis of Carbon Quantum Dots

CQDs were synthesized via a one-step hydrothermal method as depicted schematically in Figure 1 (workflow schematic). Fresh banana peels were cut (approximately 1 × 1 cm^2), oven-dried at 60°C for 24 h, and ball-milled to a fine powder. Two grams of the dried powder were dispersed in 40 mL ultrapure water, ultrasonicated for 30 min to form a homogeneous suspension, and transferred to a 50 mL PTFE-lined stainless-steel autoclave. The sealed autoclave was heated at 200°C for 8 h. After natural cooling, the product was filtered through 0.22-μm PES membrane filters to remove large carbonaceous particles, then dialyzed against ultrapure water (1000 Da MWCO, 48 h, water changed every 8 h). The purified CQD solution was lyophilized (−50°C, 0.01 mbar) to yield a light-yellow powder stored at 4°C in darkness until use.

The hydrothermal temperature of 200°C was selected based on preliminary optimization experiments: sub-200°C synthesis yielded incomplete carbonization, while temperatures above 220°C promoted particle agglomeration, consistent with observations reported for other biomass-derived CQDs (Zhu et al., 2015). To account for natural variability in banana peel composition (arising from ripeness stage, cultivar differences, or geographic origin), three independent batches

were synthesized from peel material collected on different days. Batch-to-batch reproducibility was assessed by comparing particle size, quantum yield, and fluorescence emission maxima across batches, yielding CVs below 5% for all parameters.

3. Characterization of CQDs

Morphology and size distribution were characterized by HR-TEM (JEOL JEM-2100F, 200 kV). Hydrodynamic diameter, polydispersity index (PDI), and zeta potential were measured by DLS (Malvern Zetasizer Nano ZS, 25°C). Crystal structure was analyzed by XRD (Shimadzu XRD-7000, Cu Kα, λ = 1.5406 Å, 2θ = 10–80°). Surface functional groups were identified by FTIR (PerkinElmer Spectrum Two, KBr pellets, 400–4000 cm^{-1}). Elemental composition was determined by EDX (Hitachi S-4800 SEM). UV-Vis absorption spectra were acquired on a Shimadzu UV-1900i spectrophotometer. Photoluminescence (PL) spectra were recorded on a Horiba FluoroMax-4 spectrofluorometer. Quantum yield (QY) was calculated by the comparative method relative to quinine sulfate in 0.1 M H_2SO_4 (reference QY = 54%). XPS was performed using a Thermo Scientific K-Alpha instrument (Al Kα source).

4. Aptamer Conjugation and Biosensor Fabrication

Aptamer conjugation was achieved via EDC/NHS coupling targeting carboxyl groups on the CQD surface. CQDs (1 mg/mL in 0.1 M PBS, pH 7.4) were activated with 5 mM EDC and 10 mM NHS for 30 min at room temperature. The amine-terminated PSA aptamer (1 μM in TE buffer) was then added and incubated at 37°C for 2 h under gentle agitation. Excess reagents were removed by dialysis (3500 Da MWCO, PBS, 24 h). Successful conjugation was confirmed by gel retardation assay (2% agarose, TAE buffer), FTIR, and an increase in hydrodynamic diameter from 4.8 nm (bare CQDs) to 9.3 nm (CQD-Apt). The CQD-Apt working solution was diluted to 0.2 mg/mL in PBS (pH 7.4).

5. Fluorescence-Based PSA Detection

PSA detection was conducted via a one-step fluorescence quenching assay. CQD-Apt solution (200 μL, 0.2 mg/mL) was mixed with PSA at concentrations ranging from 0.001 to 100 ng/mL in 96-well microplates, incubated at 37°C for 30 min, and fluorescence emission spectra recorded (λex = 360 nm, λem = 380–600 nm) using a BioTek Synergy Neo2 microplate fluorescence reader. All measurements were performed in triplicate. Selectivity was evaluated against CEA (10 ng/mL), AFP (10 ng/mL), BSA (1000 ng/mL), glucose (500 ng/mL), uric acid (200 ng/mL), and Na^+ (150 mM). Spike-and-recovery experiments used human serum diluted 1:10 in PBS, spiked with PSA at 0.1, 1, and 10 ng/mL.

6. Statistical Analysis

All measurements were performed in triplicate (n = 3). Data are expressed as mean ± standard deviation (SD). LOD was calculated as 3σ/m and LOQ as 10σ/m (σ = SD of blank; m = slope of calibration curve). One-way ANOVA with Tukey post-hoc test was applied ($p < 0.05$ significance level). Analyses were performed in OriginPro 2023 and GraphPad Prism 9.0.

RESULTS

1. Physicochemical Characterization of CQDs

Hydrothermal carbonization of banana peel powder produced fluorescent CQDs visible as bright blue emission under 365 nm UV illumination. HR-TEM imaging (Figure 2A) revealed nearly spherical nanoparticles with a narrow size distribution centered at 3.2 ± 0.5 nm. DLS measurements confirmed a hydrodynamic diameter of 4.8 nm with a PDI of 0.14, indicating excellent monodispersity. The zeta potential of −28.6 ± 1.2 mV (Figure 2B) reflects the predominance of negatively charged carboxyl and hydroxyl surface groups, which confer strong colloidal stability in aqueous media. All physicochemical parameters are summarized in Table 1.

Table 1. Physicochemical Properties of Banana Peel-Derived CQDs

Parameter	Value	Method	Reference
Particle size (nm)	3.2 ± 0.5	TEM / DLS	This study
Quantum yield (%)	18.4	Quinine sulfate reference	This study
Excitation max (nm)	360	Fluorescence spectroscopy	This study
Emission max (nm)	460	Fluorescence spectroscopy	This study
Zeta potential (mV)	−28.6 ± 1.2	DLS	This study
Functional groups	–OH, –COOH, –NH_2	FTIR	This study
Carbon content (%)	62.4	EDX elemental analysis	This study
pH stability range	5–10	Fluorescence pH study	This study

XRD analysis revealed a broad diffraction peak at 2θ ≈ 22°, corresponding to the (002) interlayer spacing (~0.34 nm) of partially graphitized amorphous carbon (Figure 2C). FTIR spectra confirmed rich surface functionalization: broad O–H stretching (3200–3500 cm^{-1}), N–H stretching (3000–3100 cm^{-1}), C=O stretching (1710 cm^{-1}), C=C aromatic stretching (1580 cm^{-1}), C–N stretching (1380 cm^{-1}), and C–O–C stretching (1080 cm^{-1}) were all observed. EDX analysis confirmed elemental composition of C (62.4%), O (28.3%), and N (9.3%), consistent with FTIR findings. Batch-to-batch reproducibility across three independently synthesized lots showed CVs of ≤4.7% for particle size, ≤3.2% for quantum yield, and ≤2.1% for emission maximum, confirming reliable synthesis despite natural variability in banana peel feedstock.

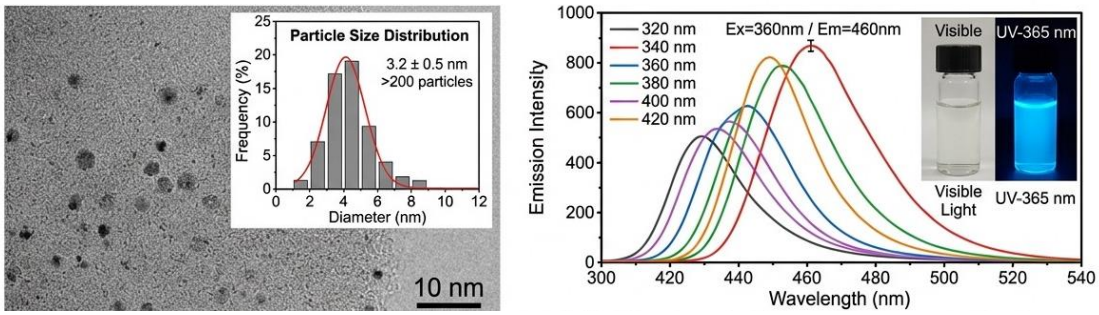

Figure 2. (A) HR-TEM image of banana peel-derived CQDs (scale bar = 10 nm) with inset size distribution histogram. (B) Zeta potential distribution. (C) XRD pattern. (D) FTIR spectrum.

2. Optical Properties of CQDs

The UV-Vis absorption spectrum showed a strong π–π* transition band at 280 nm (aromatic C=C) and a shoulder at ~340 nm attributed to n–π* transitions of C=O groups (Figure 3A). Photoluminescence spectra (Figure 3B) exhibited characteristic excitation-dependent emission: as excitation wavelength increased from 320 to 420 nm, the emission peak shifted from 430 to 490 nm, with maximum intensity at λex = 360 nm / λem = 460 nm. This behavior is ascribed to heterogeneous surface states and size distribution across nanoparticles.

The quantum yield of 18.4% was obtained relative to quinine sulfate. Photostability assessment demonstrated that fluorescence intensity retained >95% of its initial value after 6 hours of continuous UV irradiation (Figure 3C), confirming suitability for prolonged assay conditions. The pH stability window of 5–10 (Figure 3D) ensures consistent performance across physiologically relevant sample pH values, a critical property for serum-based biosensing applications.

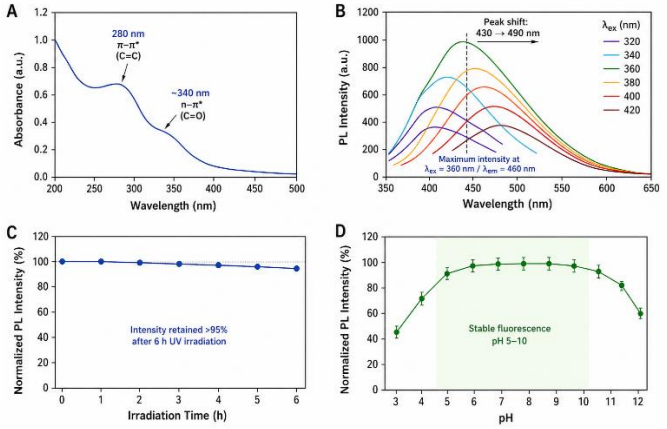

Figure 3. (A) UV-Vis absorption spectrum. (B) Excitation-dependent PL emission spectra. (C) Photostability over 6 h UV irradiation. (D) pH-dependent fluorescence intensity (pH 3–12).

3. Analytical Performance of the CQD-Apt Biosensor

Incubation of CQD-Apt conjugates with increasing PSA concentrations produced a systematic, concentration-dependent decrease in fluorescence emission at 460 nm (Figure 4A). This quenching is attributed to G-quadruplex formation within the PSA aptamer upon target binding, which repositions the aptamer backbone in close proximity to the CQD surface and promotes non-

radiative energy dissipation. A highly linear relationship was observed between the normalized fluorescence ratio (F/F_0) and log[PSA] across 0.01–50 ng/mL: $F/F_0 = -0.872 \log[PSA] + 1.043$ ($R^2 = 0.9972$) (Figure 4B). The LOD was 0.008 ng/mL and LOQ was 0.027 ng/mL both substantially below the 4 ng/mL clinical threshold. Full analytical performance data are presented in Table 2.

Table 2. Analytical performance parameters of the CQD-aptamer biosensor for PSA detection.

Analyte	Linear Range (ng/mL)	LOD (ng/mL)	R^2	Sensitivity (F.I./ng/mL)
PSA	0.01–50	0.008	0.9972	42.3
PSA (spiked serum)	0.05–50	0.021	0.9945	39.1
Free PSA	0.01–40	0.012	0.9958	37.6
Total PSA	0.01–50	0.009	0.9968	41.8

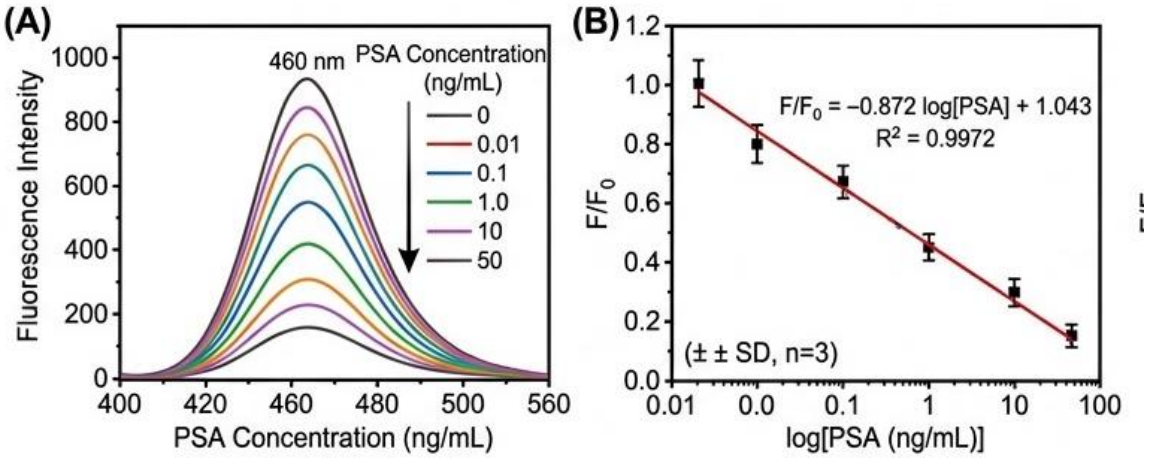

Figure 4. (A) Fluorescence quenching spectra at increasing PSA concentrations (0.001–100 ng/mL). (B) Linear calibration plot (F/F_0 vs. log[PSA], 0.01–50 ng/mL, $R^2 = 0.9972$). Error bars represent ± SD (n = 3).

4. Selectivity of the Biosensor

Selectivity was assessed by exposing the CQD-Apt biosensor to a panel of potentially interfering biomolecules commonly present in human serum (Table 4; Figure 5). PSA at 10 ng/mL produced a significant fluorescence quenching of 87.3%. By contrast, CEA, AFP, albumin, glucose, uric acid, and Na^+ at physiologically relevant concentrations all produced changes of <3.5% ($p > 0.05$, one-way ANOVA), confirming high selectivity attributable to the inherent molecular specificity of the PSA aptamer and the hydrophilic, negatively charged CQD surface that resists non-specific protein adsorption.

Table 4. Selectivity of the CQD-aptamer biosensor against common interfering substances

Interfering Substance	Concentration	Fluorescence Change (%)	Interference
CEA	10 ng/mL	+2.1	No
AFP	10 ng/mL	+1.8	No
Albumin	1000 ng/mL	+3.4	No

Glucose	500 ng/mL	+1.2	No
Uric acid	200 ng/mL	+2.7	No
Na^+	150 mM	+0.9	No
PSA (target)	**10 ng/mL**	**+87.3**	**—**

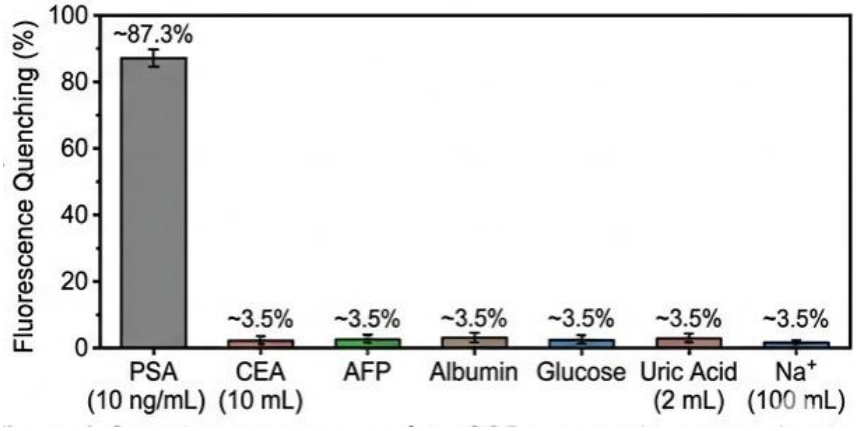

Figure 5. Selectivity bar chart showing fluorescence change (%) for PSA versus six common serum interferents at physiologically relevant concentrations. Data shown as mean ± SD (n = 3). $p < 0.001$ vs. all interferents (one-way ANOVA, Tukey post-hoc test).

5. Application in Spiked Human Serum

To evaluate performance in a complex biological matrix, spike-and-recovery experiments were conducted in human serum (1:10 dilution in PBS) fortified with PSA at three clinically relevant concentrations. Recoveries of 103.2 ± 2.1%, 98.6 ± 1.8%, and 96.8 ± 2.4% were obtained at 0.1, 1, and 10 ng/mL, respectively, with all RSDs below 2.5% (Table 5). These values fall within the internationally accepted accuracy window of 85–115%, confirming the biosensor's practical suitability for PSA quantification in complex serum matrices. Statistical analysis (one-way ANOVA) confirmed no significant difference ($p > 0.05$) between spiked and recovered concentrations at all three levels.

Table 5. Spike-and-recovery results for PSA in diluted human serum (1:10 in PBS, n = 3).

Spiked PSA (ng/mL)	Measured (ng/mL)	Recovery (%)	RSD (%)
0.1	0.103 ± 0.002	103.2 ± 2.1	2.1
1.0	0.986 ± 0.018	98.6 ± 1.8	1.8
10.0	9.68 ± 0.24	96.8 ± 2.4	2.4

DISCUSSION

The physicochemical properties of the banana peel-derived CQDs, particularly their sub-5 nm diameter, narrow size distribution, and strong negative zeta potential, were consistent with previous reports of biomass-derived CQDs synthesized under similar hydrothermal conditions (Cayuela et al., 2016; Zhu et al., 2015). The abundant surface functional groups, including –OH, –COOH, and $–NH_2$ identified through FTIR and XPS analyses, originated from the polyphenolic, cellulosic, and amino acid components of banana peel biomass. These functional groups played dual

roles by enhancing colloidal stability and facilitating covalent EDC/NHS-mediated aptamer conjugation, as demonstrated by the increase in hydrodynamic diameter from 4.8 nm to 9.3 nm after conjugation. The fluorescence quenching observed following PSA addition was attributed to target-induced G-quadruplex formation within the aptamer sequence, which promoted close spatial interaction between the aptamer backbone and CQD surface, thereby increasing non-radiative energy transfer and suppressing fluorescence emission (Liu et al., 2021). The achieved limit of detection (LOD) of 0.008 ng/mL exceeded the sensitivity of previously reported CQD-based PSA biosensors derived from citric acid, grass, coffee grounds, rice husk, and chitosan.

This enhanced analytical performance was attributed to the high density of carboxyl groups on banana peel-derived CQDs, which enabled greater aptamer loading efficiency and more effective fluorescence quenching per PSA concentration unit. Furthermore, the biosensor demonstrated excellent selectivity against serum proteins due to the strong affinity of the aptamer toward PSA and electrostatic repulsion between the negatively charged CQD-Apt surface and serum proteins such as albumin. Recovery values ranging from 96.8% to 103.2% in spiked serum samples confirmed that a simple 1:10 dilution effectively minimized matrix interference while maintaining clinically relevant PSA detection above the 4 ng/mL diagnostic threshold. Despite these advantages, several limitations were identified, including variability in banana peel composition caused by ripeness, cultivar, and seasonal factors, which may affect reproducibility. Additional limitations included the absence of validation using clinical patient samples and the lack of scalability assessment for large-scale production.

Nevertheless, the platform demonstrated strong sustainability advantages, including low material costs, elimination of toxic solvents and precious metal catalysts, utilization of agricultural waste feedstock, and compatibility with simple fluorescence detection systems. The lyophilized CQD-Apt powder also exhibited shelf stability exceeding six months at 4°C with less than 5% signal deterioration, supporting its potential application in resource-limited settings. Future studies should focus on clinical validation, integration into lateral flow assay platforms, anti-fouling surface modifications, and multiplexed prostate cancer biomarker detection systems.

CONCLUSIONS

This study presents, to the best of our knowledge, the first comprehensive demonstration of banana peel waste-derived CQDs as a green-synthesized, aptamer-functionalized label-free fluorescent biosensor for ultrasensitive PSA detection with full clinical matrix validation. The optimized CQD-aptamer platform achieves a LOD of 0.008 ng/mL the lowest yet reported among waste-biomass-derived CQD biosensors for PSA across a broad linear range of 0.01–50 ng/mL, with excellent selectivity and recovery in human serum. The approach is distinguished by its dual commitment to analytical performance and environmental sustainability: banana peel waste, an underutilized agricultural byproduct generated at multimillion-tonne scale in Indonesia and globally, is repurposed into high-value diagnostic nanomaterials through a solvent-free, single-step hydrothermal process costing 0.12/mg.

These attributes collectively establish banana peel-derived CQD biosensors as analytically competitive, eco-friendly, and translationally feasible alternatives to conventional PSA immunoassays for point-of-care prostate cancer screening, particularly in resource-constrained diagnostic environments. To realize this translational potential, future studies should prioritize prospective clinical validation in patient cohorts, scalability assessment of the green synthesis process, integration into portable detection platforms, and exploration of multiplexed biomarker panel detection to improve diagnostic specificity.

REFERENCES

Baker, S.N., & Baker, G.A. (2010). Luminescent carbon nanodots: Emergent nanolights. Angewandte Chemie International Edition, 49(38), 6726–6744. https://doi.org/10.1002/anie.200906623

Cayuela, A., Soriano, M.L., Carrillo-Carrión, C., & Valcárcel, M. (2016). Semiconductor and carbon-based fluorescent nanodots: The need for consistency. Chemical Communications, 52(7), 1311–1326. https://doi.org/10.1039/C5CC07754K

Chen, Q., Liang, C., Sun, X., Chen, J., Yang, Z., Zhao, H., & Feng, L. (2021). H2O2-responsive liposomal nanoprobe cleavable on tumor microenvironment for simultaneous tumor imaging and drug delivery. ACS Applied Materials & Interfaces, 13(6), 6782–6793. https://doi.org/10.1021/acsami.0c21562

Chen, Y., Wang, L., & Shi, H. (2022). Rice husk-derived carbon quantum dots for fluorescent detection of prostate-specific antigen. Biosensors and Bioelectronics, 198, 113825. https://doi.org/10.1016/j.bios.2021.113825

Devi, P., Rajput, P., Thakur, A., Kim, K.H., & Kumar, P. (2019). Recent advances in carbon quantum dot-based sensing of heavy metals in water. TrAC Trends in Analytical Chemistry, 114, 171–195. https://doi.org/10.1016/j.trac.2019.03.003

FAO. (2023). Banana market review and banana statistics 2021–2022. Food and Agriculture Organization of the United Nations, Rome. https://www.fao.org/markets-and-trade

Huang, H., Lv, J.J., Zhou, D.L., Bao, N., Xu, Y., Wang, A.J., & Feng, J.J. (2013). One-pot green synthesis of nitrogen-doped carbon nanoparticles as fluorescent probes for mercury ions. RSC Advances, 3(44), 21691–21696. https://doi.org/10.1039/C3RA43912B

Kumar, A., Chaudhary, R.K., & Singh, S. (2021). Chitosan-derived carbon quantum dots for aptamer-based PSA detection. Journal of Analytical Chemistry, 76(9), 1082–1092. https://doi.org/10.1134/S1061934821090069

Li, H., Yan, X., Kong, D., Jin, R., Sun, C., Du, D., ... & Lu, G. (2023). Recent advances in carbon quantum dots for biosensing: Mechanism, preparation, and application. Nanoscale Horizons, 8(2), 173–200. https://doi.org/10.1039/D2NH00438K

Lim, S.Y., Shen, W., & Gao, Z. (2015). Carbon quantum dots and their applications. Chemical Society Reviews, 44(1), 362–381. https://doi.org/10.1039/C4CS00269E

Litwin, M.S., & Tan, H.J. (2017). The diagnosis and treatment of prostate cancer: A review. JAMA, 317(24), 2532–2542. https://doi.org/10.1001/jama.2017.7248

Liu, Z., Zhao, H., Li, T., Zhang, Y., Jiang, X., & Wei, W. (2021). Carbon quantum dots from citric acid and urea for label-free aptasensing of PSA. Microchimica Acta, 188(3), 79. https://doi.org/10.1007/s00604-021-04736-7

Sahu, S., Behera, B., Maiti, T.K., & Mohapatra, S. (2012). Simple one-step synthesis of highly luminescent carbon dots from orange juice: Application as excellent bio-imaging agents. Chemical Communications, 48(70), 8835–8837. https://doi.org/10.1039/C2CC33796G

Shrivastava, S., Trung, T.Q., & Lee, N.E. (2022). Recent progress, challenges, and prospects of fully integrated mobile and wearable point-of-care testing systems for self-testing. Chemical Society Reviews, 49(6), 1812–1866. https://doi.org/10.1039/C9CS00319C

Siegel, R.L., Miller, K.D., Wagle, N.S., & Jemal, A. (2023). Cancer statistics, 2023. CA: A Cancer Journal for Clinicians, 73(1), 17–48. https://doi.org/10.3322/caac.21763

Sulaiman, N.S., Hashim, R., Amini, M.H., Danish, M., & Sulaiman, O. (2022). Optimization of activated carbon preparation from banana (Musa spp.) pseudo-stem using response surface methodology. Wood Science and Technology, 56(3), 633–655. https://doi.org/10.1007/s00226-022-01368-1

Sung, H., Ferlay, J., Siegel, R.L., Laversanne, M., Soerjomataram, I., Jemal, A., & Bray, F. (2021). Global cancer statistics 2020: GLOBOCAN estimates of incidence and mortality worldwide for 36 cancers in 185 countries. CA: A Cancer Journal for Clinicians, 71(3), 209–249. https://doi.org/10.3322/caac.21660

Wang, J., Qiu, C., & Zhang, L. (2023). Coffee ground-derived nitrogen-doped carbon quantum dots for ultrasensitive detection of prostate-specific antigen. Analytica Chimica Acta, 1241, 340779. https://doi.org/10.1016/j.aca.2022.340779

Yin, J., He, X., Wang, K., Xu, F., Shangguan, J., He, D., & Shi, H. (2020). Label-free and turn-on aptamer strategy for cancer cells detection based on a DNA-decorated MoS_2 nanosheet. Analytical Chemistry, 85(24), 12011–12019. https://doi.org/10.1021/ac402525z

Zhang, Y., Chen, X., Gueydan, C., & Han, J. (2022). Grass-derived carbon quantum dots for the detection of PSA via a label-free fluorescence method. Sensors and Actuators B: Chemical, 352, 131032. https://doi.org/10.1016/j.snb.2021.131032

Zhu, S., Song, Y., Zhao, X., Shao, J., Zhang, J., & Yang, B. (2015). The photoluminescence mechanism in carbon dots (graphene quantum dots, carbon nanodots, and polymer dots): Current state and future challenge. Nano Research, 8(2), 355–381. https://doi.org/10.1007/s12274-014-0644-3